Supplementary Material

Molecular Mechanisms of 33-mer Gliadin Peptide Oligomerisation

María Julia Amundarain[1], María Georgina Herrera[2] Fernando Zamarreño[1], Juan Francisco Viso[1], Marcelo D. Costabel[1#], Verónica I. Dodero[2#]

1 Grupo de Biofísica, Instituto de Física del Sur, Universidad Nacional del Sur, Bahía Blanca, Buenos Aires, Argentina

2. Universität Bielefeld, Fakultät für Chemie, Organische Chemie, Universitätsstr. 25, 33615 Bielefeld, Germany.

corresponding authors:

veronica.dodero@uni-bielefeld.de; costabel@criba.edu.ar

Methods

Table S1. Details of the molecular dynamics simulations.

Number of peptides	Box vectors ℓ [nm]	Box angles [°]	Volume of the box [nm^3]	Water molecules per box	Ions per box	Simulation Times [ns]
1	13.1	60 60 90	1611	52021	146	250
2	13.5	60 60 90	1727	56784	156	250
3	13.0	60 60 90	1538	50104	139	250
4	13.0	60 60 90	1538	49898	139	250
10 - 1	17.7	60 60 90	3903	127335	353	250
10 - 2	20.7	60 60 90	6289	207356	568	100

Table S2. Initial distance between peptides in the MD simulations.

Number of peptides	Distance between the centers of mass of the peptides [Å]	Distance between the centers of mass of the closest residues [Å]
2	15.2	10.1
3	25.9	11.0
4	21.4	9.4

Decamer – Atomistic simulations

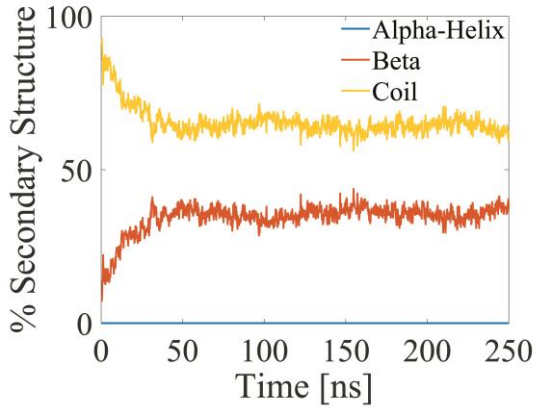

Figure S1. The evolution of the secondary structure as a function of simulation time evidences the increment of beta content. The PPII structure is computed as a coil in this model.

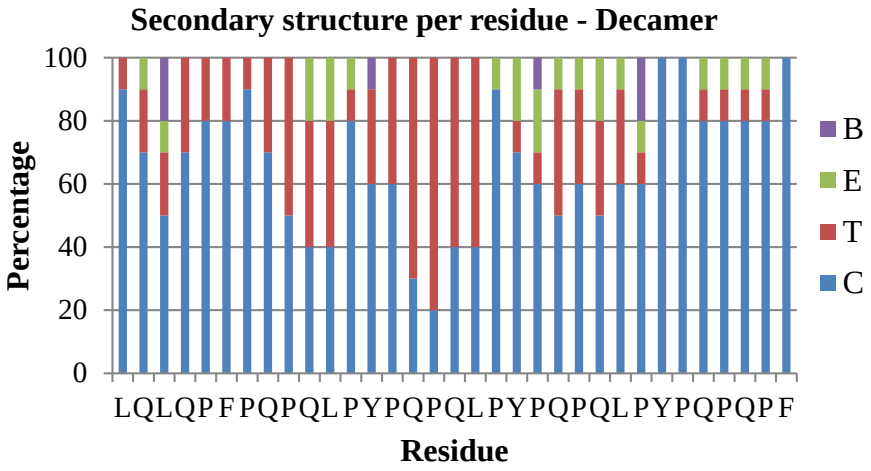

Figure S2. Secondary structure per residue of 33-mer decamer extracted from the representative conformation of the first 100 ns of simulation, calculated with STRIDE. Beta-like structures: Isolated bridge (B), Extended strand (E) and Turn (T). The PPII structure (C) is computed in the coils group, as described in the Methods section (coils are all secondary structures which are not beta-like, alpha-helices, 3-10 helices or pi-helices).

We performed a second atomistic simulation of ten monomers in solution (Fig. 3S). The monomers formed an octamer, and two monomers remained isolated. The monomers remained elongated during the first nanoseconds. The formation of the octamer was stepwise, the first five monomers aggregate in the first nanoseconds, and a sixth monomer was included after 30 ns. Meanwhile a dimer was also formed. The same dimer aggregated with the hexamer and formed an octamer. The number of H-bonds presents a lineal increase during the first 30 ns (Fig.3S-F), showing the evolution of the formation of the oligomers, which is also presented as a decrease in the SAS (Fig.3S-G).

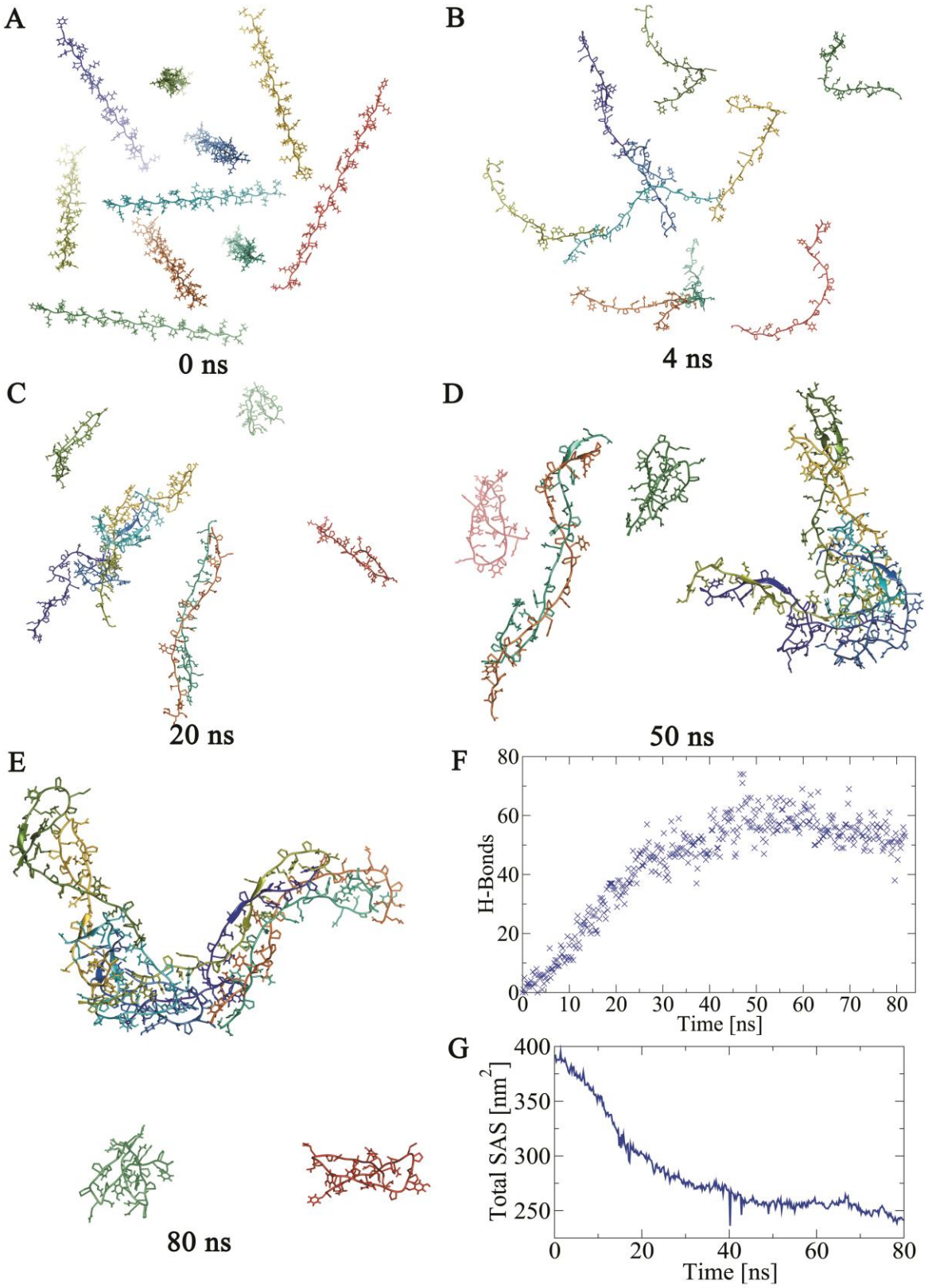

Figure S3. (A) The first frame of the simulation presents the 10 monomers in elongated conformations. (B) In the first frames of the simulation, the monomers begin to interact with each other. (C) The first noticeable aggregation step is the formation of a pentamer

and a dimer. (D) At 50 ns different aggregates can be found including a hexamer and a dimer. (E) At 80 ns an octamer is found together with two isolated monomers. (F) The lineal increase in the number of H-bonds is compatible with aggregation. (G) The SAS decreases in agreement with the oligomerisation process.

Decamer – Coarse-Grained simulations

The coarse-grained MD simulations were also performed with the GROMACS 4.6.5 package [1,2] using the SIRAH force field and the WT4 representation [3] of water molecules. The conditions of this simulation were the same as those specified for atomistic simulations except for the time step, which was increased to 20 fs and the use of V-rescale thermostat. The protocol consisted of energy minimization with Steepest Descent algorithm to a maximum force of 10 kJ/mol.nm and then a 5 ns position restrained equilibration on the NPT ensemble. Finally a 1 μs production simulation was performed. The results were analysed with SIRAH tools [4].

In this simulation; a decamer was formed by the approach of the monomers in the first nanoseconds of the entire production run (1 μs). The structure obtained for the aggregate was initially loose and elongated, and it eventually formed a more compact structure (Figure S4A). The solvent-accessible area showed a plateau after 300 ns, which accounts for the stability of the compaction of the aggregate (Figure S4B). Moreover, during this simulation, the PPII content decreased to lower values until it reached about 50% of the total secondary structures (Figure S4C). Thus an increase of the β structure is observed.

The implementation of a CG scheme on the aggregation of peptides has been employed and reviewed, particularly for smaller peptides [5,6]. However, the comparison of these results with the atomistic approach requires careful interpretation. Firstly, the beads used to represent groups of atoms retain only the main features of the residues. Secondly, the resulting structures with simplified interactions, also have fewer degrees of freedom than the atomistic simulations. Therefore the conformational space explored is not the same. Finally, it is hypothesised that, at this scale, aggregates do not exist in a single form, but instead present different structures compatible with further aggregation. This would account for the differences between the atomistic and coarse-grained decamers.

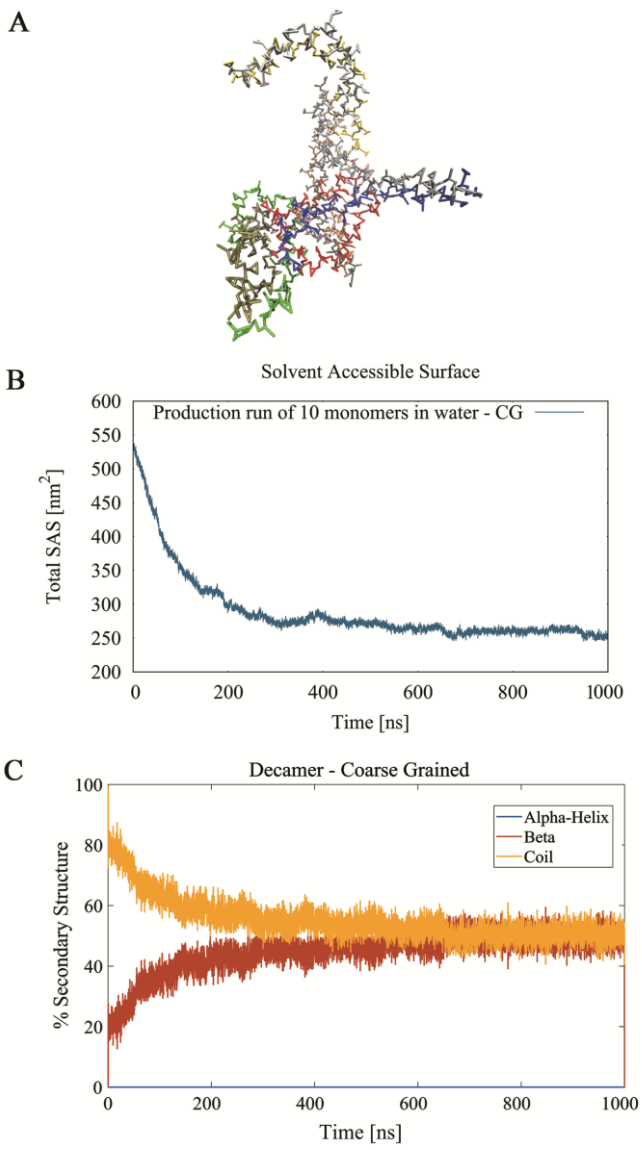

Figure S4. (A) Final structure of the decamer obtained from 1 μs coarse-grained MD simulations. (B) The Solvent Accessible Surface decreased due to the formation of the decamer. (C) The beta content was increased during the simulation, while the percentage of coil structures diminished until both reached ~50%. PPII structure is computed as a coil in this model.

Monomer

Table S3. Variation of the electrostatic energy with pH of 33-mer monomer.

pH	Average Electrostatic energy (10^4 kJ/mol)
7	2.20 ± 0.05
2	2.27 ± 0.05
9	2.25 ± 0.04

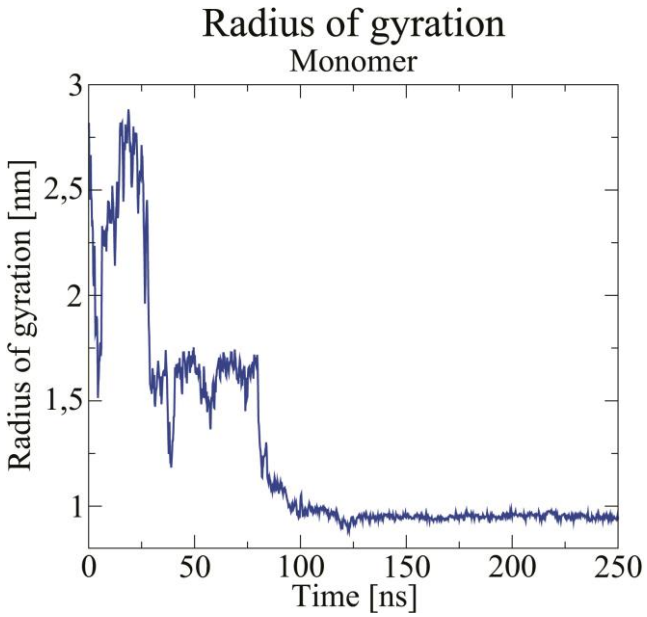

Figure S5. Structural evolution of the monomer showing the three stages of folding through the radius of gyration.

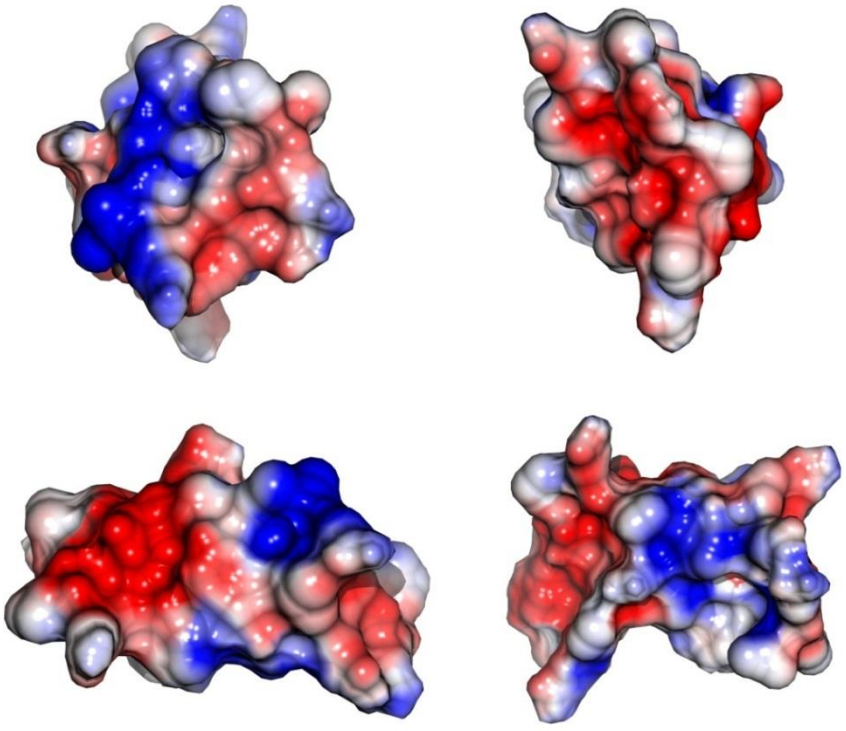

Figure S6. Different views of the molecular surface of the folded monomer (100 ns) coloured by the electrostatic potential. It shows the amphiphilic characteristic of this peptide. Blue surfaces correspond to $1k_BT/e$ ($4.3\ 10^{-21}$ J/e) and red surfaces to $-1k_BT/e$.

Dimer

Table S4. A network of H-bonds stabilizes the structure of the most representative conformation of the dimer (81 ns).

Donor	Acceptor
LEU 1.A N	PHE 33.B O2
LEU 3.A N	GLN 31.B O
GLN 4.A NE2	PRO 28.B O
GLN 10.A NE2	TYR 20.B OH
LEU 11.A N	PRO 9.A O
TYR 13.A N	LEU 11.A O
GLN 15.A N	TYR 13.A O
GLN 15.A NE2	TYR 27.B OH
GLN 17.A N	GLN 15.A OE1
GLN 17.A NE2	LEU 25.B O
LEU 18.A N	PRO 23.B O
GLN 22.A N	LEU 18.B O
GLN 22.A NE2	PRO 23.A O
GLN 24.A N	GLN 17.B OE1
GLN 31.A N	PRO 5.B O
GLN 2.B NE2	PHE 33.A O2
GLN 10.B N	PRO 26.A O
GLN 15.B NE2	PRO 14.B O
GLN 17.B N	GLN 15.B O
LEU 18.B N	GLN 22.A O
LEU 25.B N	PRO 16.A O
GLN 31.B N	LEU 3.A O
PHE 33.B N	LEU 1.A O

Table S5. A network of H-bonds stabilizes the structure of the representative conformation of the dimer in the second cluster (227 ns).

Donor	Acceptor
LEU 3.A N	GLN 31.B O
GLN 4.A NE2	TYR 27.B OH
LEU 18.A N	PRO 23.B O
GLN 24.A N	TYR 13.B O
GLN 24.A NE2	GLN 15.B O
GLN 24.A NE2	GLN 17.B OE1
GLN 2.B N	PHE 33.A O2
GLN 10.B N	PRO 26.A O
TYR 13.B N	GLN 24.A O
GLN 15.B N	GLN 22.A O
GLN 17.B N	GLN 22.A OE1
LEU 18.B N	GLN 22.A OE1
LEU 25.B N	PRO 16.A O

TYR 27.B OH	PRO 5.A O
GLN 31.B N	LEU 3.A O
PHE 33.B N	LEU 1.A O

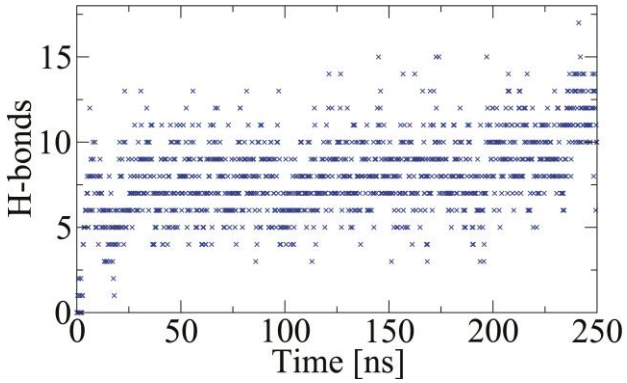

Figure S7. H-bonds increased during the simulation of the dimer as a consequence of the oligomerization process.

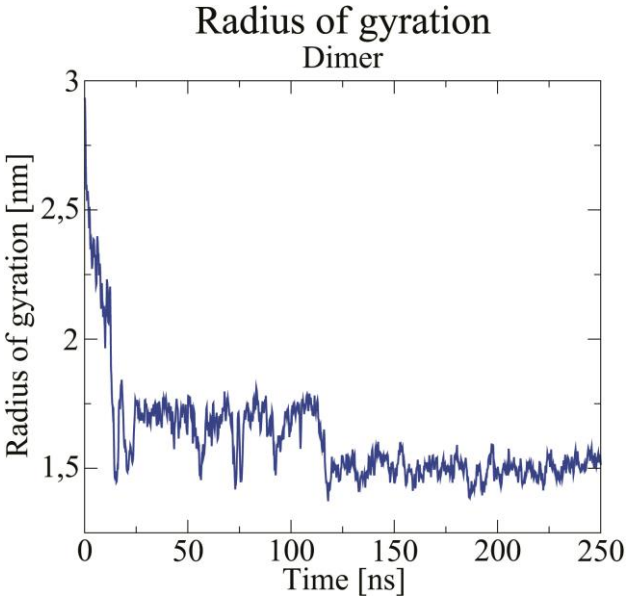

Figure S8. The radius of gyration of the MD simulations of the dimer show the initial approach of the monomers, the formation of the dimer and then the different degrees of elongation.

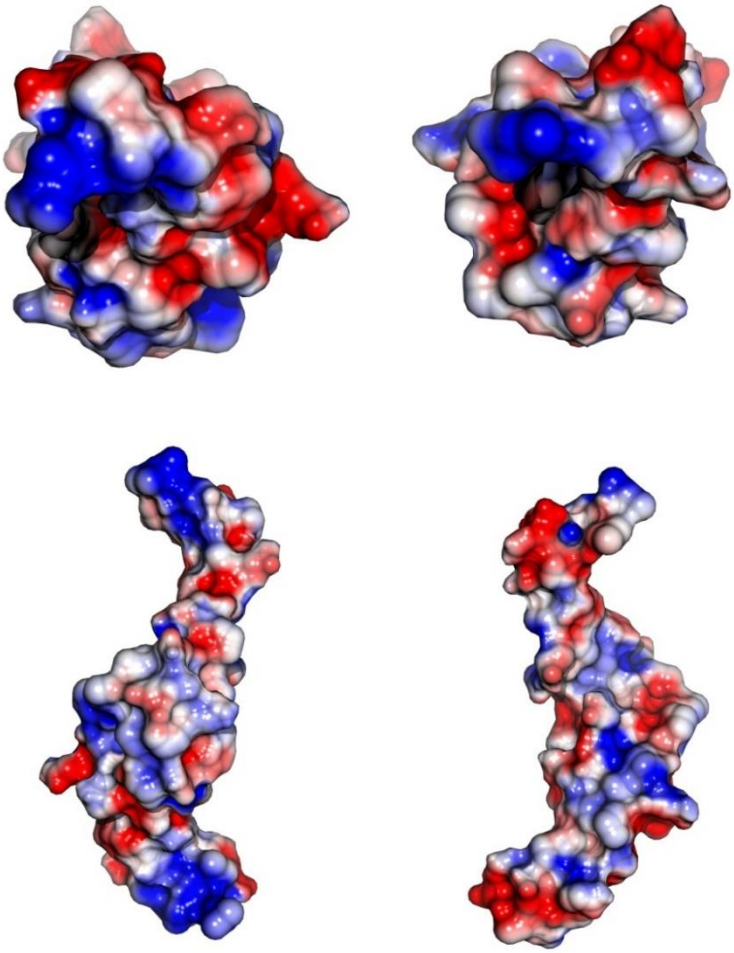

Figure S9. Views from different orientations of the molecular surface of the dimer at 100 ns coloured by the electrostatic potential. The dimer retains its amphiphilic characteristic.

Trimer

Table S6. A network of H-bonds stabilizes the structure of the representative conformation of the stabilised trimer (203 ns).

Donor	Acceptor	Donor	Acceptor
LEU 3.A N	GLN 31.B O	TYR 20.B OH	PRO 32.C O
GLN 10.A N	GLN 10.C OE1	GLN 22.B N	GLN 2.C O
GLN 10.A NE2	LEU 11.C O	GLN 24.B N	GLN 4.C O
LEU 18.A N	PRO 23.B O	LEU 25.B N	PRO 16.A O
GLN 22.A N	LEU 18.B O	GLN 31.B N	LEU 3.A O
GLN 24.A N	GLN 17.B OE1	PHE 33.B N	LEU 1.A O
TYR 27.A OH	PRO 30.C O	GLN 2.C N	GLN 22.B OE1
GLN 29.A N	GLN 17.C OE1	GLN 4.C N	GLN 22.B O
GLN 29.A NE2	GLN 17.C OE1	PHE 6.C N	GLN 24.B O
GLN 31.A N	PRO 5.B O	GLN 15.C N	GLN 8.B O
GLN 2.B N	GLN 24.C OE1	TYR 20.C N	GLN 29.A OE1
GLN 4.B N	LEU 25.C O	GLN 24.C N	GLN 4.B OE1
GLN 4.B NE2	GLN 31.A O	LEU 25.C N	GLN 2.B O
GLN 4.B NE2	TYR 20.C OH	TYR 27.C N	GLN 4.B O
GLN 8.B N	GLN 15.C OE1	GLN 31.C NE2	GLN 22.A OE1
GLN 17.B N	GLN 22.A O	GLN 31.C NE2	PRO 19.B O
LEU 18.B N	GLN 22.A O		

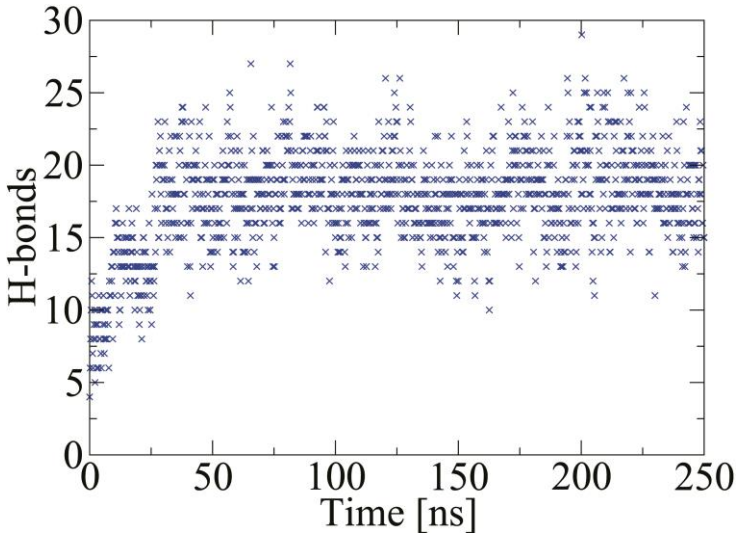

Figure S10. The trimer is stabilised by an increasing number of H-bonds formed during the oligomerisation process.

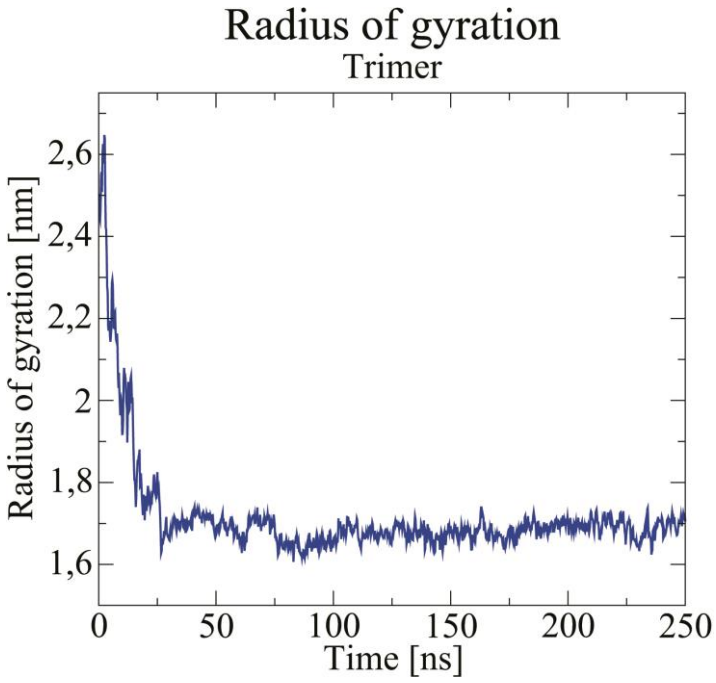

Figure S11. The radius of gyration of the MD simulations of the trimer shows the initial approach of the monomer and dimer, the formation of the trimer and the stability of the obtained structure after 30ns.

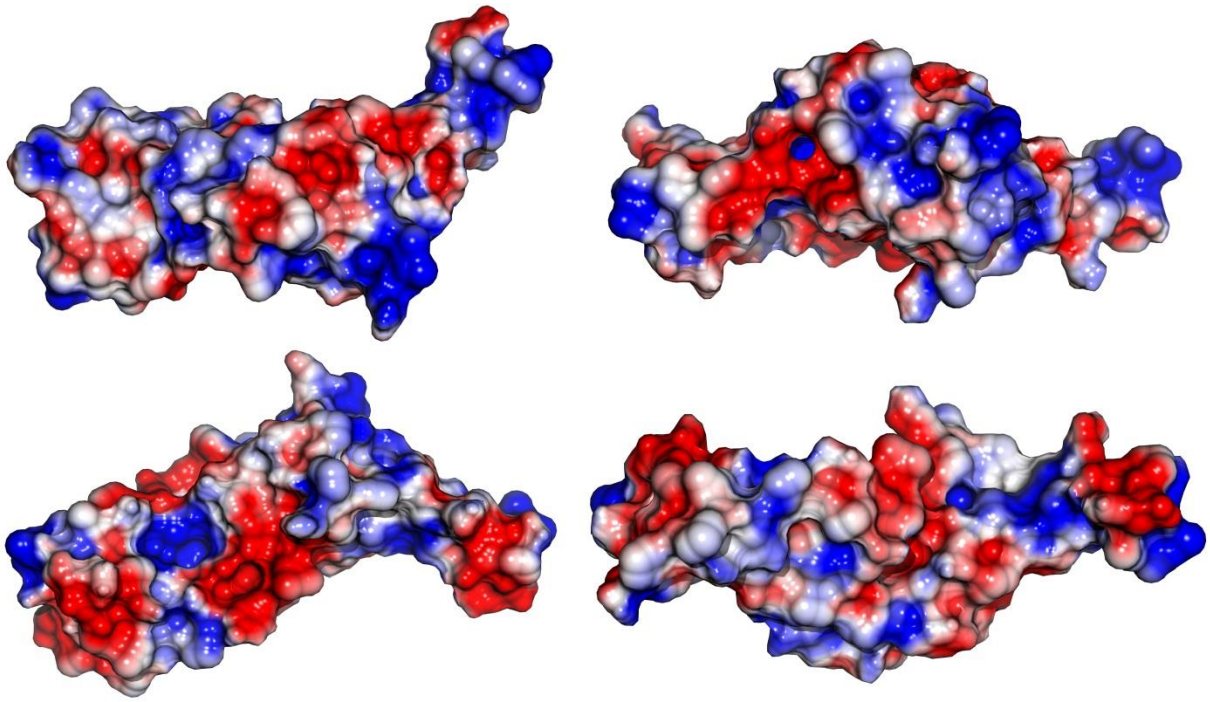

Figure S12. Views from different orientations of the molecular surface of the trimer at 100ns (in the converged region of the RMSD) coloured by the electrostatic potential.

Tetramer

Table S7. A network of H-bonds stabilizes the structure of the most representative conformation of the tetramer (152 ns).

Donor	Acceptor	Donor	Acceptor
GLN 2.A N	PHE 33.D O2	GLN 24.B NE2	GLN 17.A OE1
LEU 3.A N	GLN 31.B O	LEU 25.B N	PRO 16.A O
GLN 4.A NE2	TYR 27.B OH	GLN 31.B N	LEU 3.A O
GLN 4.A NE2	PRO 28.B O	PHE 33.B N	LEU 1.A O
GLN 10.A N	GLN 10.C OE1	GLN 4.C N	GLN 22.B O
LEU 18.A N	PRO 23.B O	PHE 6.C N	GLN 24.B O
GLN 22.A N	LEU 18.B O	GLN 10.C NE2	TYR 20.B OH
GLN 22.A NE2	PRO 30.C O	GLN 15.C NE2	GLN 2.D O
GLN 24.A N	GLN 17.B OE1	TYR 20.C N	GLN 29.A OE1
GLN 24.A NE2	GLN 17.D OE1	GLN 24.C NE2	GLN 2.B OE1
LEU 25.A N	GLN 29.C OE1	TYR 27.C OH	GLN 10.D O
GLN 29.A N	GLN 17.C OE1	GLN 29.C NE2	LEU 25.A O
GLN 31.A N	PRO 5.B O	GLN 29.C NE2	TYR 27.A OH
GLN 2.B N	GLN 24.C OE1	GLN 31.C NE2	GLN 22.A OE1
GLN 4.B NE2	TYR 20.C OH	GLN 31.C NE2	PRO 19.B O
GLN 8.B N	GLN 15.C OE1	TYR 20.D N	GLN 17.B O
LEU 18.B N	GLN 22.A O	GLN 22.D NE2	PRO 19.A O
TYR 20.B OH	PRO 32.C O	GLN 31.D N	GLN 4.A OE1
GLN 22.B NE2	GLN 2.C O	PHE 33.D N	GLN 2.A O
GLN 24.B N	GLN 4.C O		

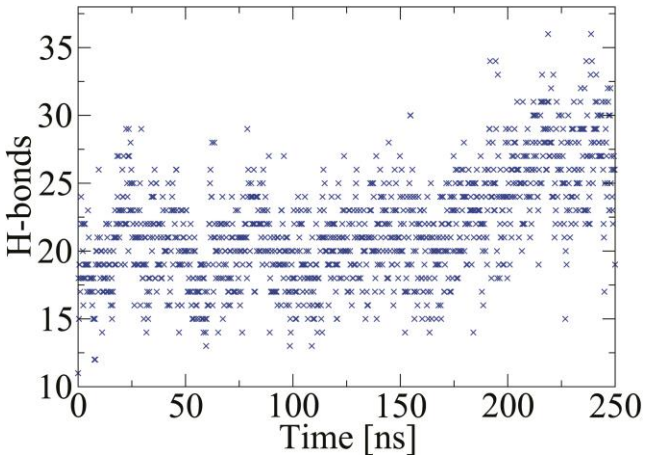

Figure S13. The number of H-bonds in the simulation of a trimer and a monomer is another manifestation that aggregation into a tetramer has occurred.

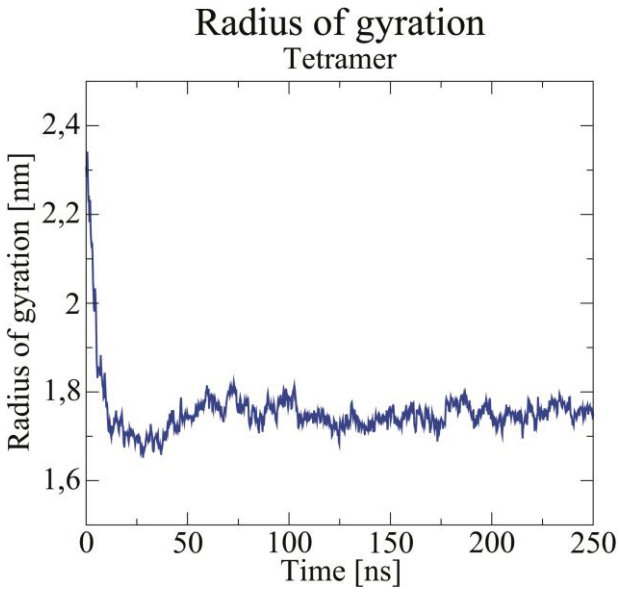

Figure S14. The radius of gyration of the MD simulations of the tetramer represents the fast oncoming of the trimer and monomer and the resultant stable tetramer.

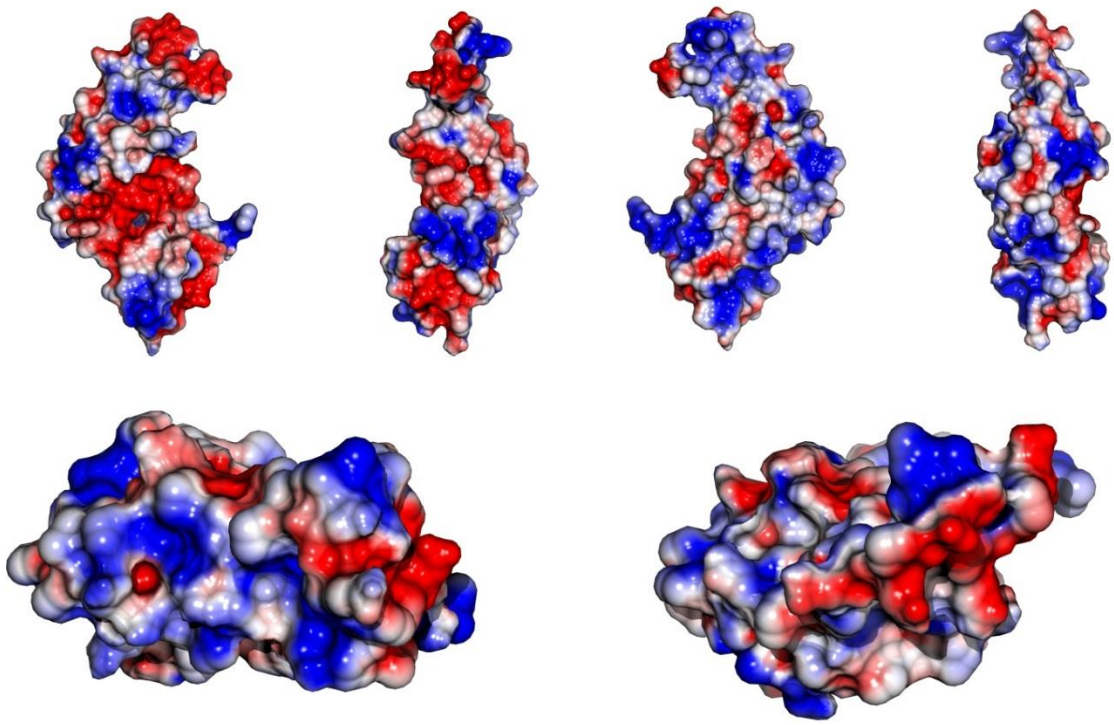

Figure S15. Views from different orientations of the molecular surface of the tetramer (at 100ns, after reaching the convergence of the simulation) coloured by the electrostatic potential.

Evolution of the secondary structures

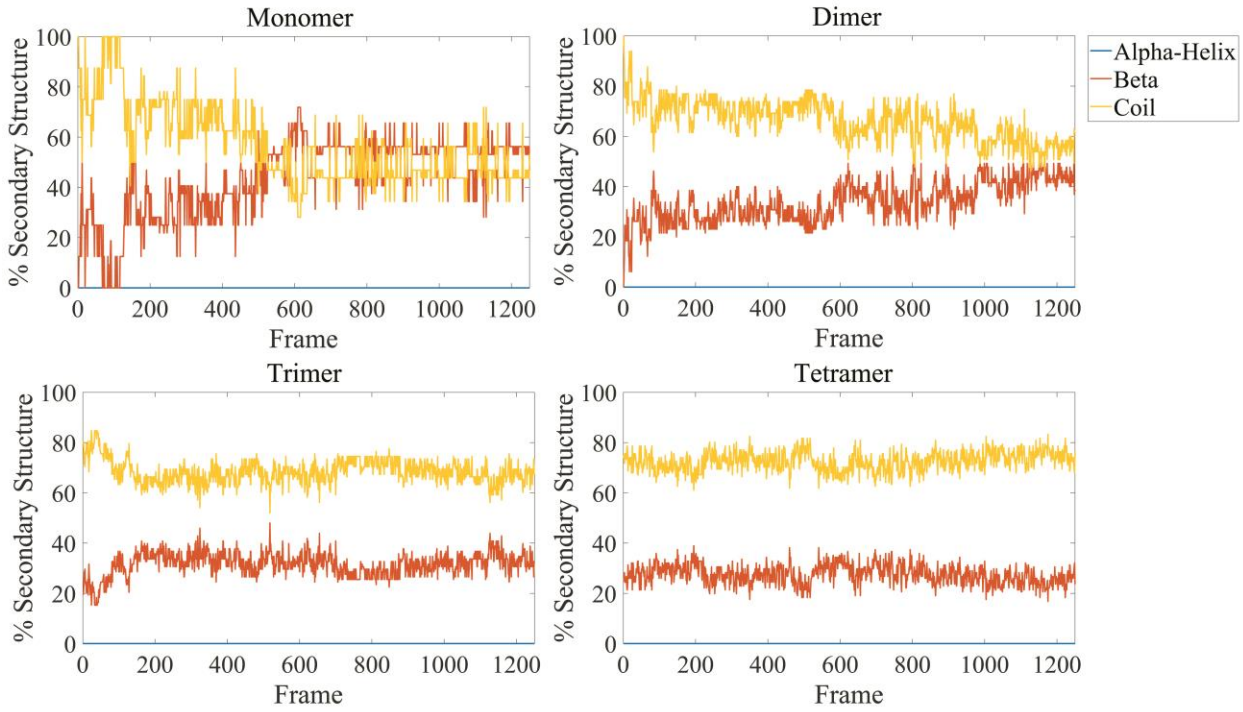

Figure S16. The evolution of the secondary structure during the MD simulations shows a similar trend for all the oligomers. During the first 250ns in both atomistic and coarse-grained simulations coil structures represent around 70% of the total secondary structures. While the values for alpha-helices remained zero in all the MD simulations, the content of beta structures was increased.

Dityrosines

We selected from visual inspection of the trajectories of the MD simulations, those tyrosines that were close enough to form a dityrosine-bond potentially. The distances between the CZ atoms of the selected residues are plotted.

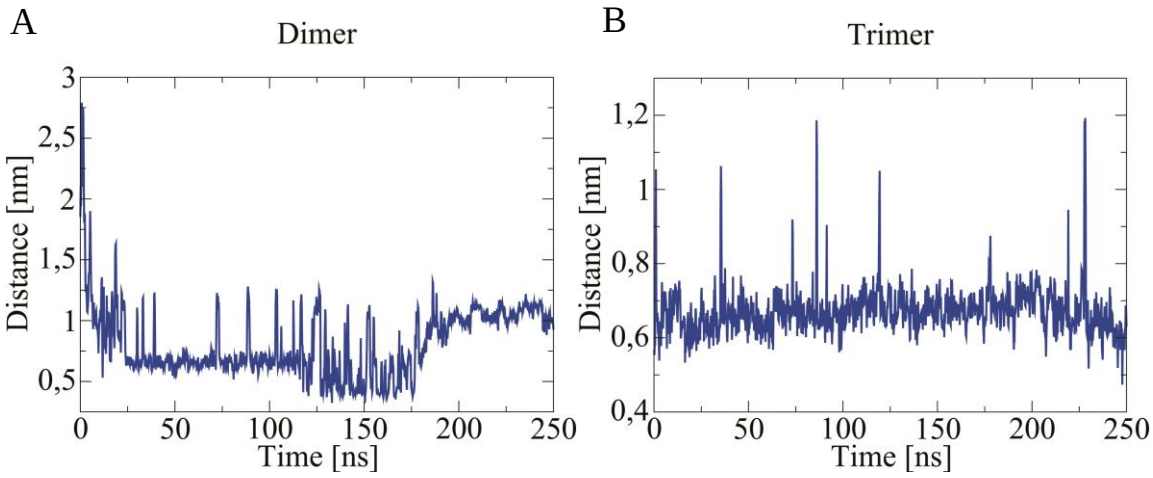

Figure S17. Distance between CZ atoms of Tyr69 and Tyr76 of chains A and B in the dimer (A) and trimer (B).

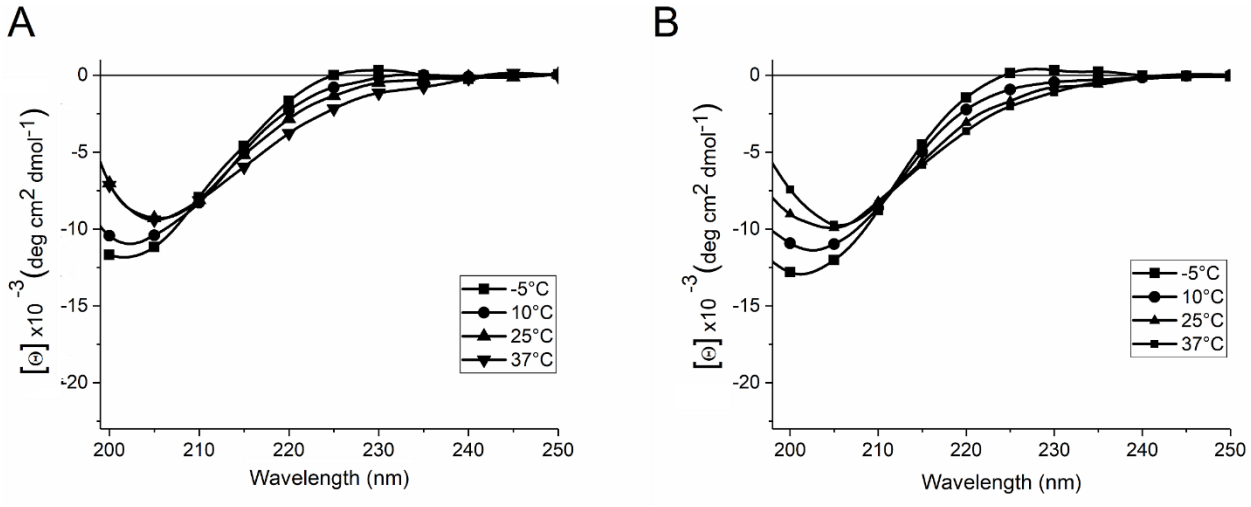

Figure S18: Circular dichroism temperature-dependent spectra of 33-mer peptide at 50 µM in absence of the peroxidase enzyme under different experimental conditions. A) In 10 mM phosphate 150 mM NaCl pH 7.4; B) in 100 mM borate buffer pH 8.8.

Determination of the molecular mass of the oligomers detected by gel electrophoresis.

To determine the Molecular mass of the oligomers and define which are the species detected, we used Image J software. In this case, we compared the mobility of the molecular marker with the samples and by this analysis, we obtained which oligomers were present.

A

Molecular Mass Marker	Distance
3,5	52
6,5	65
14	103
17	132
26	185

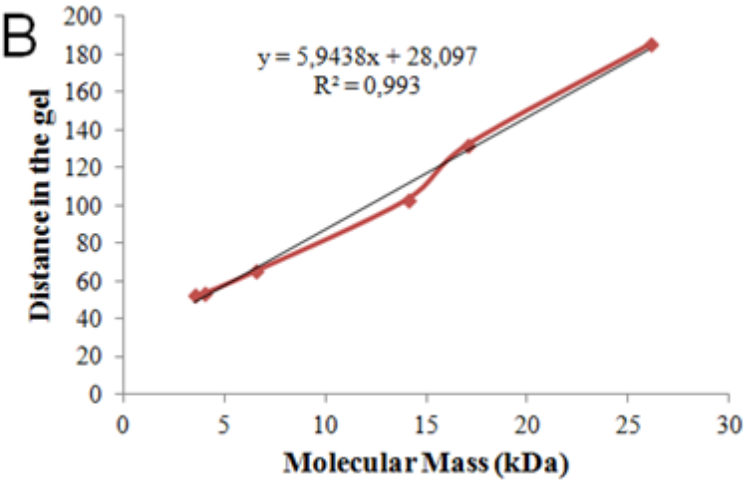

C

Molecular Mass Marker	Distance
10	106
15	153
20	186
25	216
37	262
50	299

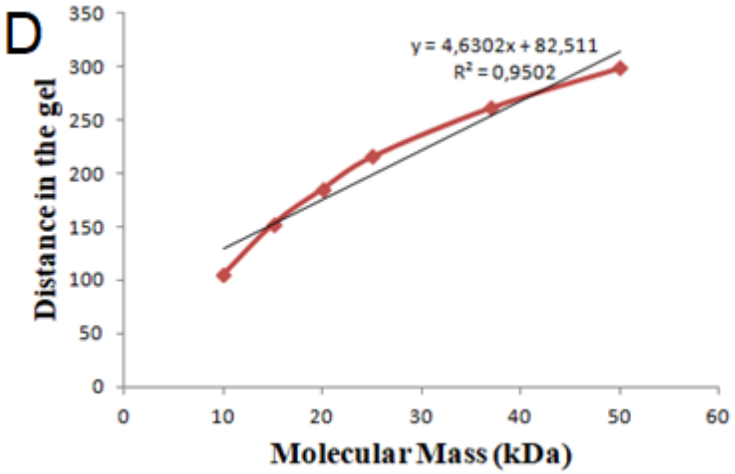

Figure S19. (A) Table showing the molecular mass of the different proteins contained in the low molecular mass marker and the distance mobility of each band. (B) The plot of mass versus distance mobility obtained by the data presented in the A showing the values of the parameters obtained of the curve by linear fitting. (C) Table showing the molecular mass of the different proteins contained in the high molecular mass marker and the distance mobility of each band. (D) The plot of mass versus distance mobility obtained by the data presented in the C showing the values of the parameters obtained of the curve by linear fitting. The references used for the distance determination of both markers was lowest and finishing part of the gel.

A

Distance oligomers 20 minutes	Molecular Mass oligomers	Number of Monomers
57	4,9	1,22
70	7,0	1,76
94	11,1	2,77

B

Distance oligomers 1 Hour	Molecular Mass oligomers	Number of Monomers
55	4,5	1,13
77	8,2	2,06
95	11,3	2,81
115	14,6	3,66
147	20,0	5,00

C

Distance oligomers after 1 hour	Molecular mass of the oligomers	Number of monomers
191	23,430737	6,01
210	27,534232	7,06
220	29,693966	7,61
240	34,013434	8,72

Figure S20. Tables showing the distance, molecular mass and number of monomers estimated for the low mass oligomers detected using the data obtained with the markers showed in Figures S12 A and B .(A) Time 20 minutes and (B) Time 1 hour. (C) The same but analysing the bigger oligomers, using the high molecular mass marker presneted in S12 C and D.

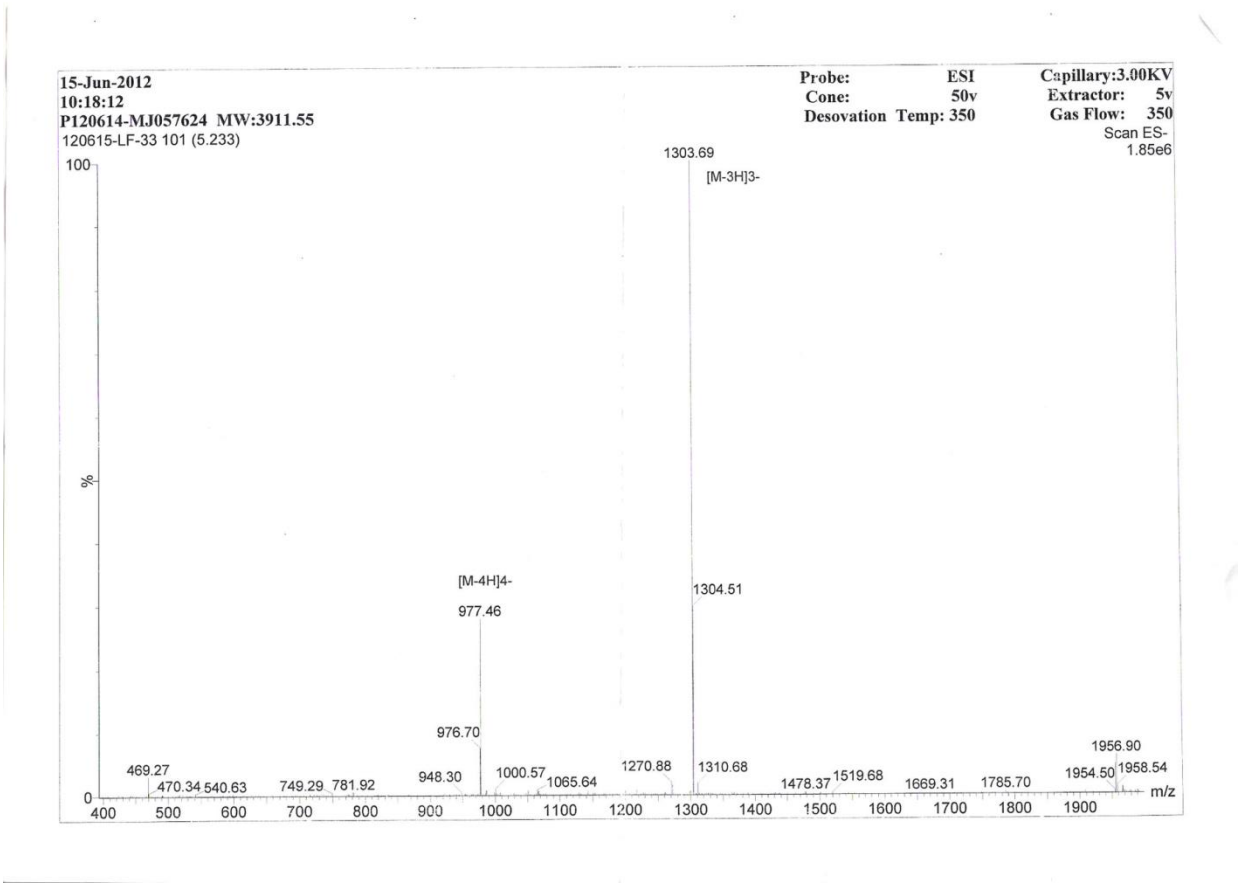

Figure S21. ESI-Mass Spectra of 33-mer gliadin peptide

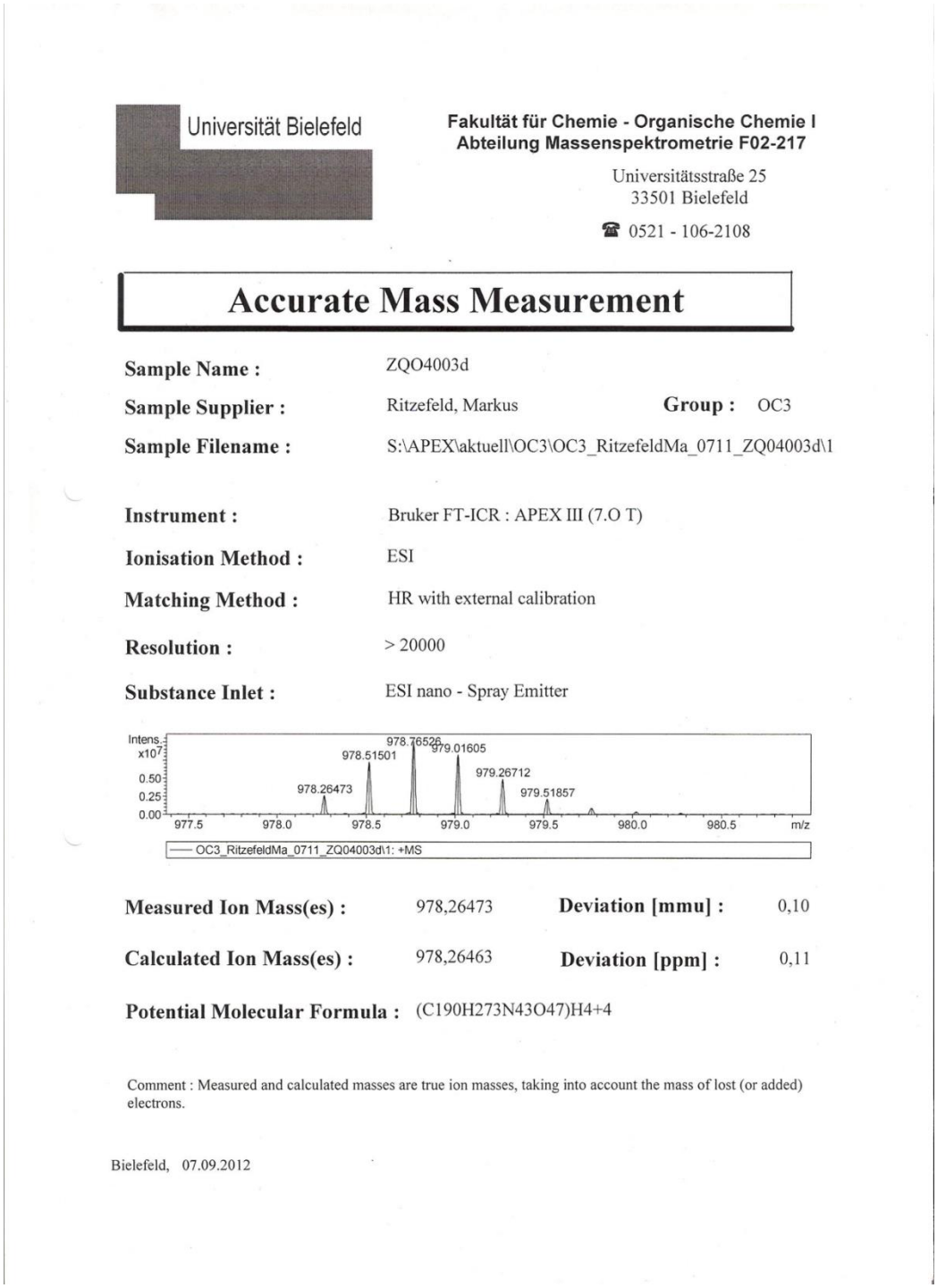

Universität Bielefeld

Fakultät für Chemie - Organische Chemie I
Abteilung Massenspektrometrie F02-217

Universitätsstraße 25
33501 Bielefeld

☎ 0521 - 106-2108

Accurate Mass Measurement

Sample Name : ZQO4003d

Sample Supplier : Ritzefeld, Markus **Group :** OC3

Sample Filename : S:\APEX\aktuell\OC3\OC3_RitzefeldMa_0711_ZQ04003d\1

Instrument : Bruker FT-ICR : APEX III (7.O T)

Ionisation Method : ESI

Matching Method : HR with external calibration

Resolution : > 20000

Substance Inlet : ESI nano - Spray Emitter

Measured Ion Mass(es) : 978,26473 **Deviation [mmu] :** 0,10

Calculated Ion Mass(es) : 978,26463 **Deviation [ppm] :** 0,11

Potential Molecular Formula : (C190H273N43O47)H4+4

Comment : Measured and calculated masses are true ion masses, taking into account the mass of lost (or added) electrons.

Bielefeld, 07.09.2012

Figure S22. Accurate-Mass-analysis

References

1. Berendsen HJC, van der Spoel D, van Drunen R. GROMACS: A message-passing parallel molecular dynamics implementation. *Comput. Phys. Commun.* 91(1–3), 43–56 (1995).

2. Páll S, Abraham MJ, Kutzner C, Hess B, Lindahl E. Tackling Exascale Software Challenges in Molecular Dynamics Simulations with GROMACS [Internet]. In: *Solving Software Challenges for Exascale: International Conference on Exascale Applications and Software, EASC 2014, Stockholm, Sweden, April 2-3, 2014, Revised Selected Papers*. Markidis S, Laure E (Eds.). . Springer International Publishing, Cham, 3–27 (2015). Available from: https://doi.org/10.1007/978-3-319-15976-8_1.

3. Darré L, Machado MR, Dans PD, Herrera FE, Sergio P. Another Coarse Grain Model for Aqueous Solvation: WAT FOUR ? *J. Chem. Theory Comput.* 6(12), 3793–3807 (2010).

4. Machado MR, Pantano S. SIRAH tools: mapping, back mapping and visualisation of coarse-grained models. *Bioinformatics*. 32(10), 1568–1570 (2016).

5. Wang Y, Voth GA. Molecular dynamics simulations of polyglutamine aggregation using solvent-free multiscale coarse-grained models. *J. Phys. Chem. B*. 114(26), 8735–8743 (2010).

6. Morriss-Andrews A, Shea JE. Simulations of protein aggregation: Insights from atomistic and coarse-grained models. *J. Phys. Chem. Lett.* 5(11), 1899–1908 (2014).